

Electronic Supplementary Information for

A general dual-templating approach to biomass-derived hierarchically porous heteroatom-doped carbon materials for enhanced electrocatalytic oxygen reduction

Xiaoge Li,^{‡a} Bu Yuan Guan,^{‡b} Shuyan Gao,^{*a} and Xiong Wen (David) Lou^{*b}

^a School of Chemistry and Chemical Engineering, Henan Normal University, Xinxiang Henan 453007, P.R. China. E-mail: shuyangao@htu.cn

^b School of Chemical and Biomedical Engineering, Nanyang Technological University, 62 Nanyang Drive, Singapore, 637459, (Singapore) Email: xwlou@ntu.edu.sg; davidlou88@gmail.com
Webpage: <http://www.ntu.edu.sg/home/xwlou/>

[‡] These two authors contribute equally to this work.

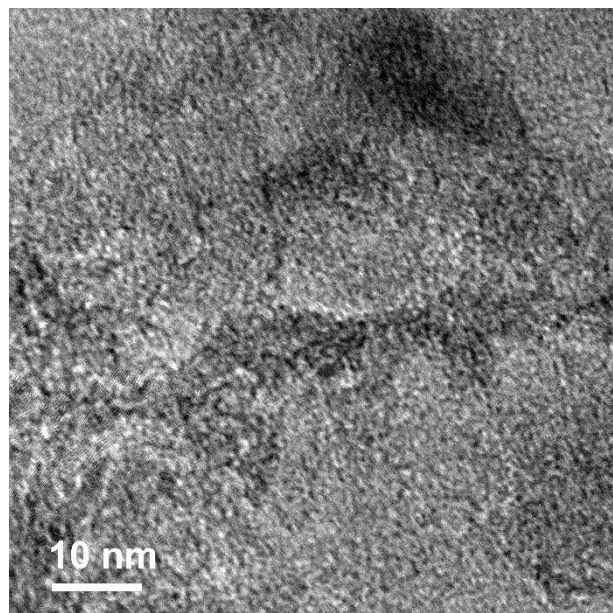


Fig. S1 High-resolution TEM image of $\text{N}_{0.54}\text{-Z}_3\text{/M}_1\text{-900}$.

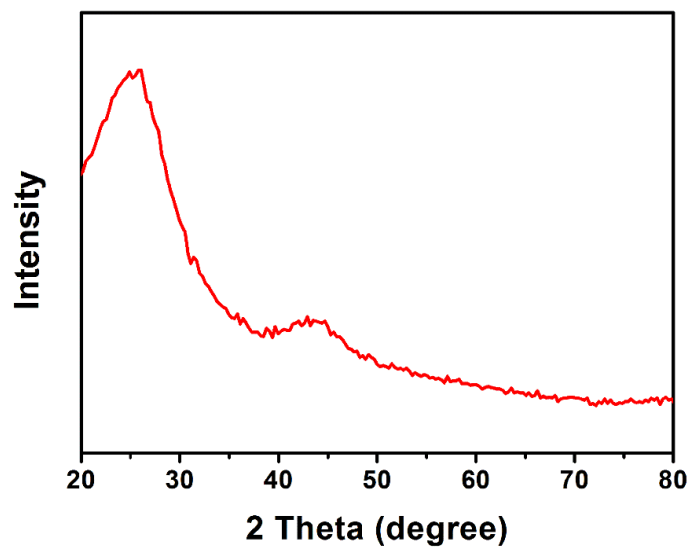


Fig. S2 XRD pattern of $\text{N}_{0.54}\text{-Z}_3\text{/M}_1\text{-900}$.

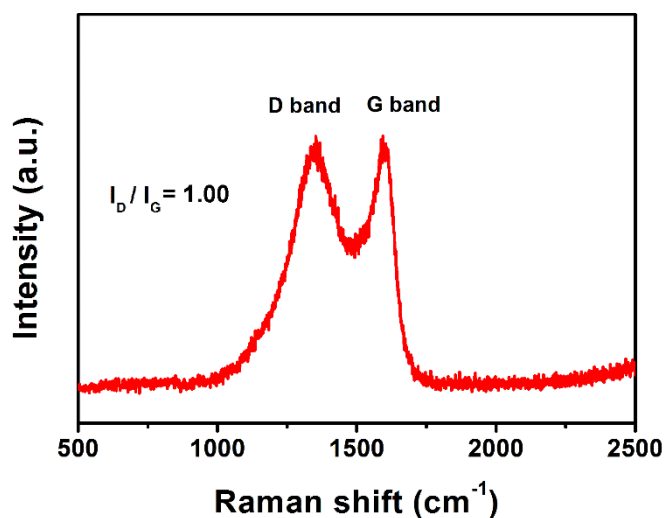


Fig. S3 Raman spectrum of $\text{N}_{0.54}\text{-Z}_3\text{/M}_1\text{-900}$.

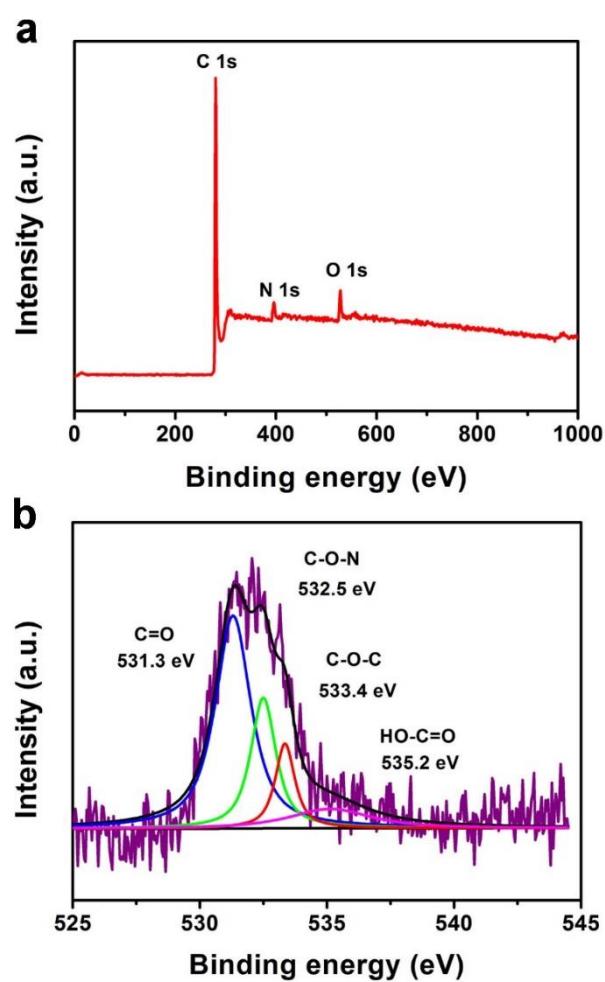


Fig. S4 (a) XPS survey and (b) O 1s spectra of $\text{N}_{0.54}\text{-Z}_3\text{/M}_1\text{-900}$.

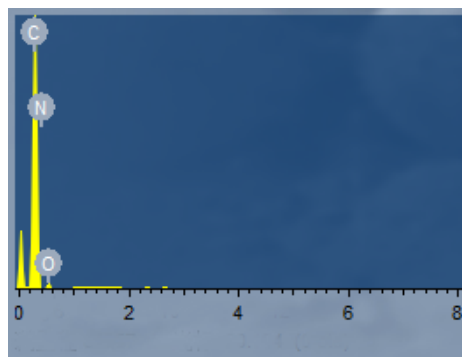


Fig. S5 EDX spectrum of $\text{N}_{0.54}\text{-Z}_3\text{/M}_1\text{-900}$.

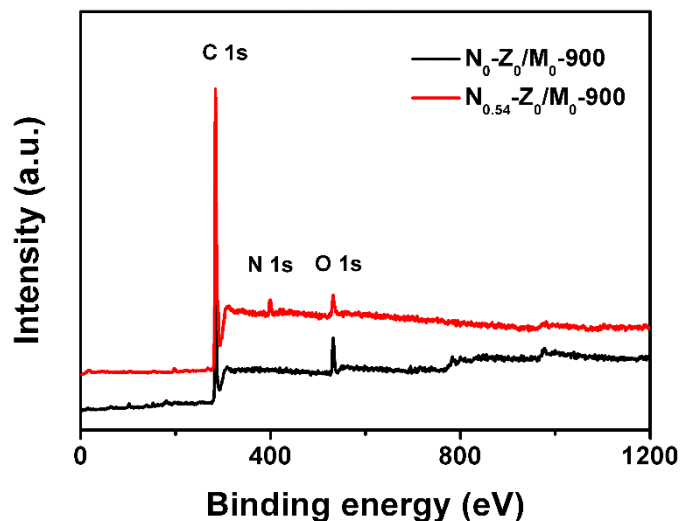


Fig. S6 XPS survey spectra of $\text{N}_0\text{-Z}_0\text{/M}_0\text{-900}$ and $\text{N}_{0.54}\text{-Z}_0\text{/M}_0\text{-900}$.

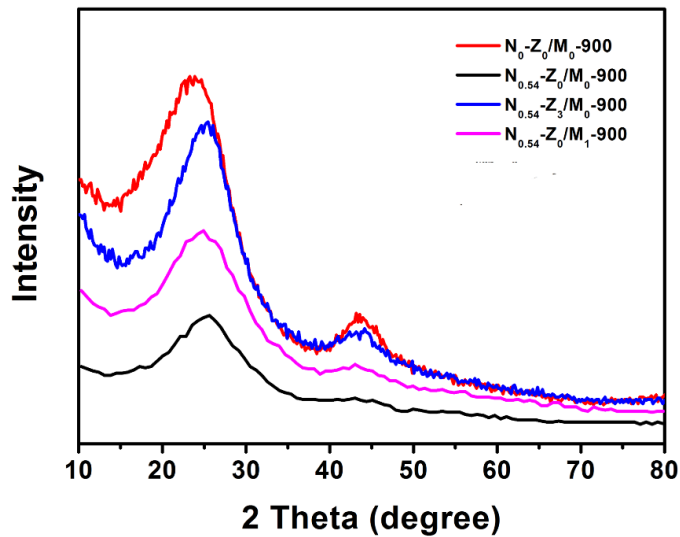


Fig. S7 XRD patterns of $N_0\text{-}Z_0/\text{M}_0\text{-}900$, $N_{0.54}\text{-}Z_0/\text{M}_0\text{-}900$, $N_{0.54}\text{-}Z_0/\text{M}_1\text{-}900$ and $N_{0.54}\text{-}Z_3/\text{M}_0\text{-}900$.

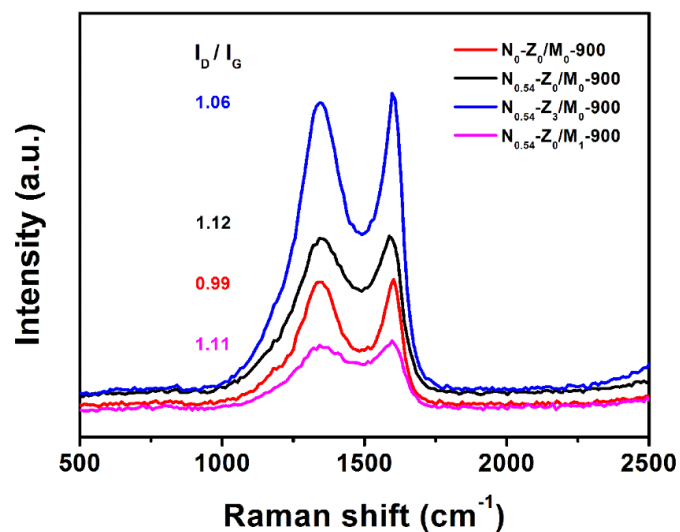


Fig. S8 Raman spectra of $N_0\text{-}Z_0/\text{M}_0\text{-}900$, $N_{0.54}\text{-}Z_0/\text{M}_0\text{-}900$, $N_{0.54}\text{-}Z_0/\text{M}_1\text{-}900$ and $N_{0.54}\text{-}Z_3/\text{M}_0\text{-}900$.

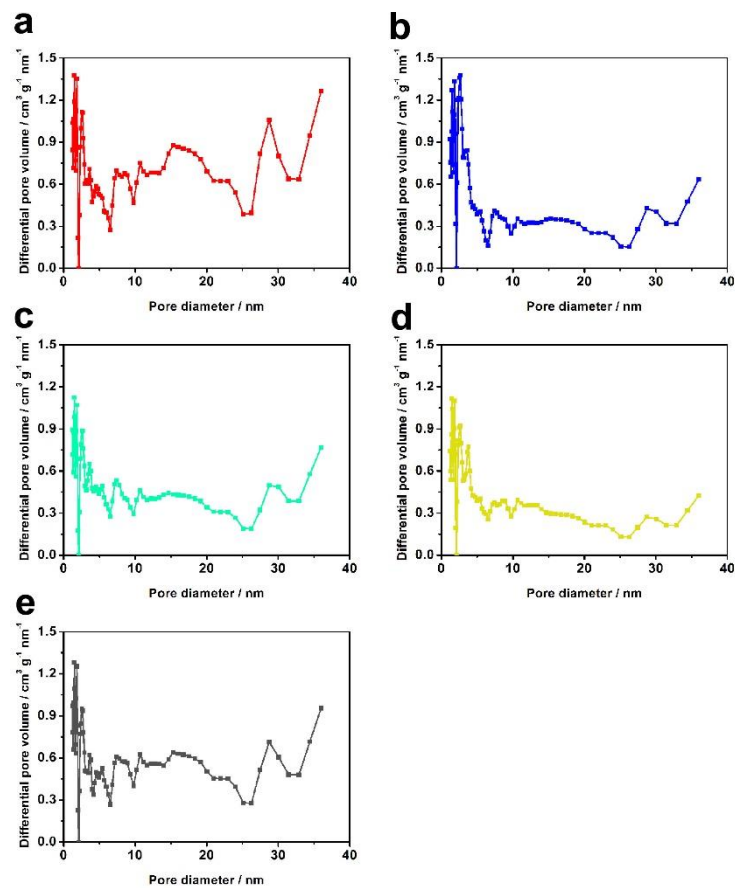


Fig. S9 Pore size distributions of hierarchically porous heteroatom-doped carbon materials derived from (a) carrots, (b) Chinese yam stems, (c) ginkgo leaves, (d) tung flowers, and (e) long beans.

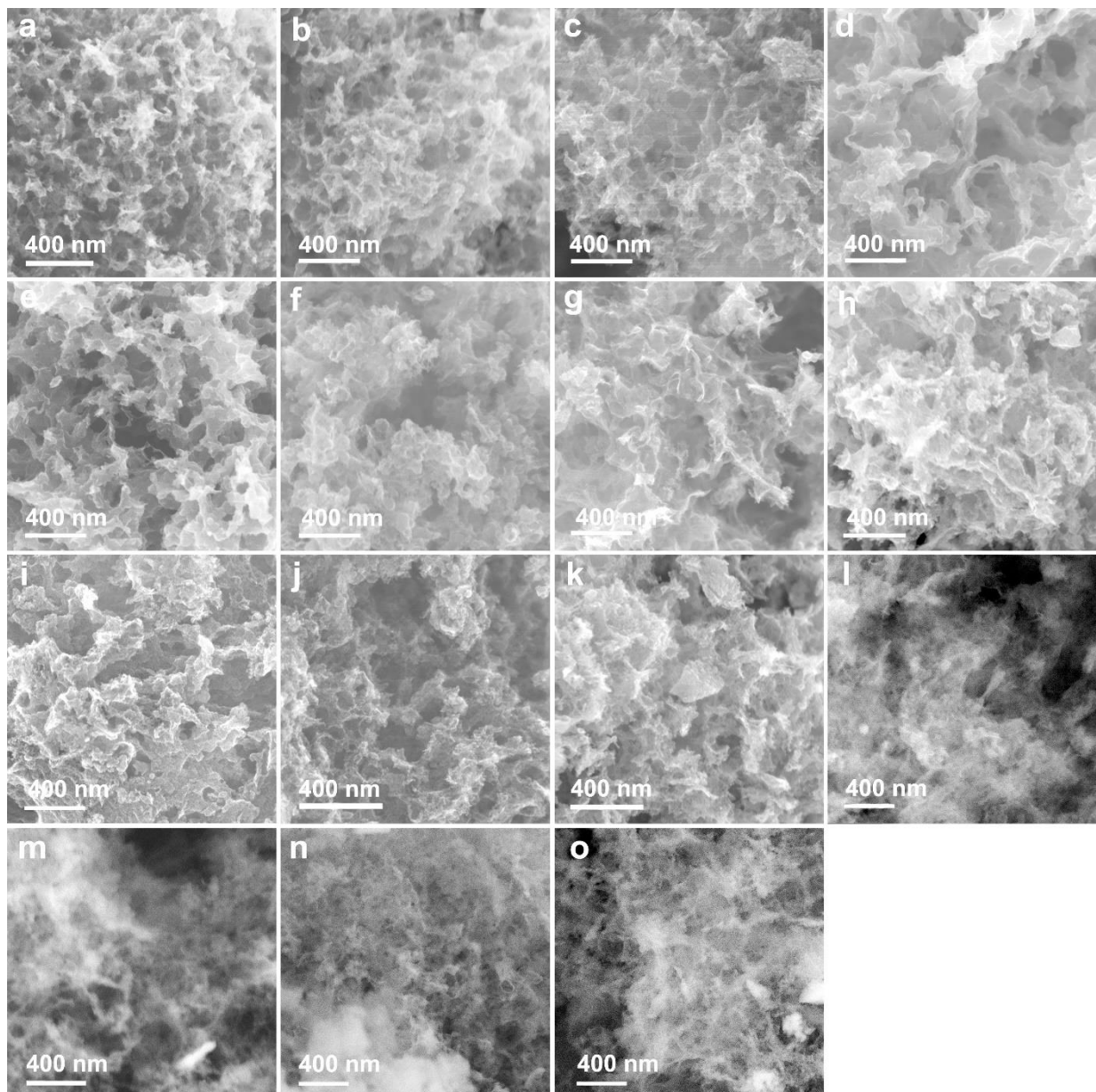


Fig. S10 FESEM images of hierarchically porous heteroatom-doped carbon materials derived from (a) cirsium setosum leaves, (b) lavender flowers, (c) mother chrysanthemum leaves, (d) stigma of corn, (e) bamboo fungus, (f) felon herb, (g) rabdosia rubescens stems, (h) rhus typhina fruit, (i) kowkui leaves, (j) loofah fruit, (k) mother chrysanthemum flowers, (l) peanut leaves, (m) honeysuckle flowers, (n) chili and (o) malachium aquaticum leaves.

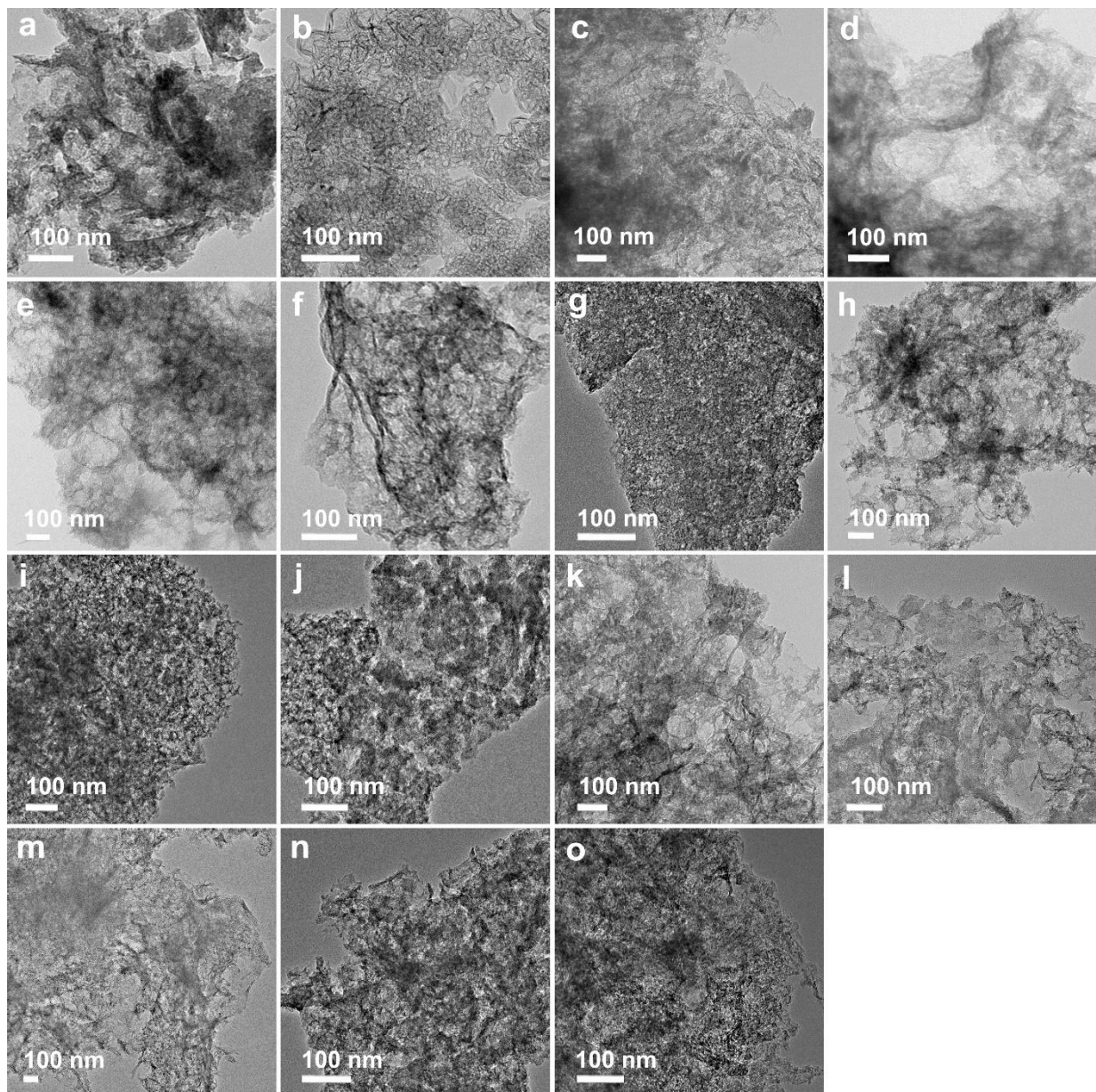


Fig. S11 TEM images of hierarchically porous heteroatom-doped carbon materials derived from (a) cirsium setosum leaves, (b) lavender flowers, (c) mother chrysanthemum leaves, (d) stigma of corn, (e) bamboo fungus, (f) felon herb, (g) rabdosia rubescens stems, (h) rhus typhina fruit, (i) kowkui leaves, (j) loofah fruit, (k) mother chrysanthemum flowers, (l) peanut leaves, (m) honeysuckle flowers, (n) chili and (o) malachium aquaticum leaves.

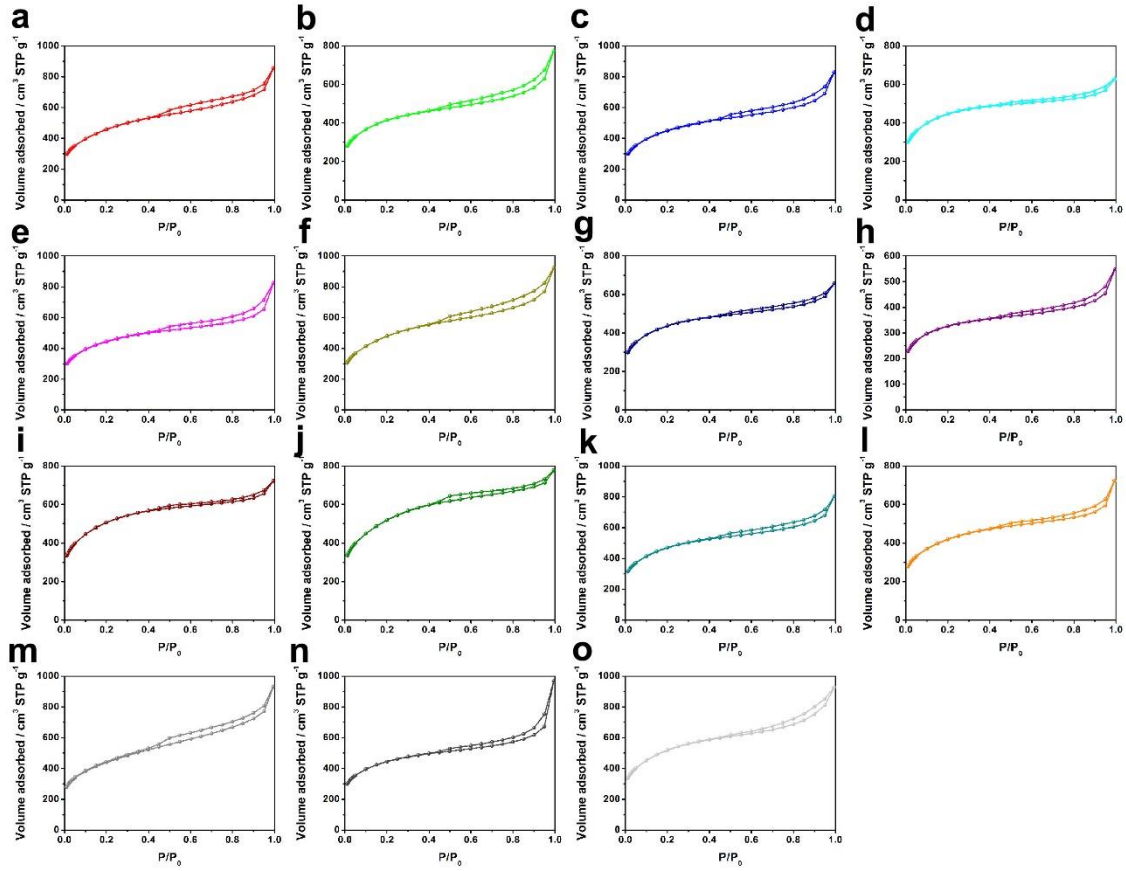


Fig. S12 N_2 sorption isotherms of hierarchically porous heteroatom-doped carbon materials derived from (a) cirsium setosum leaves, (b) lavender flowers, (c) mother chrysanthemum leaves, (d) stigma of corn, (e) bamboo fungus, (f) felon herb, (g) rhabdosia rubescens stems, (h) rhus typhina fruit, (i) kowkui leaves, (j) loofah fruit, (k) mother chrysanthemum flowers, (l) peanut leaves, (m) honeysuckle flowers, (n) chili and (o) malachium aquaticum leaves.

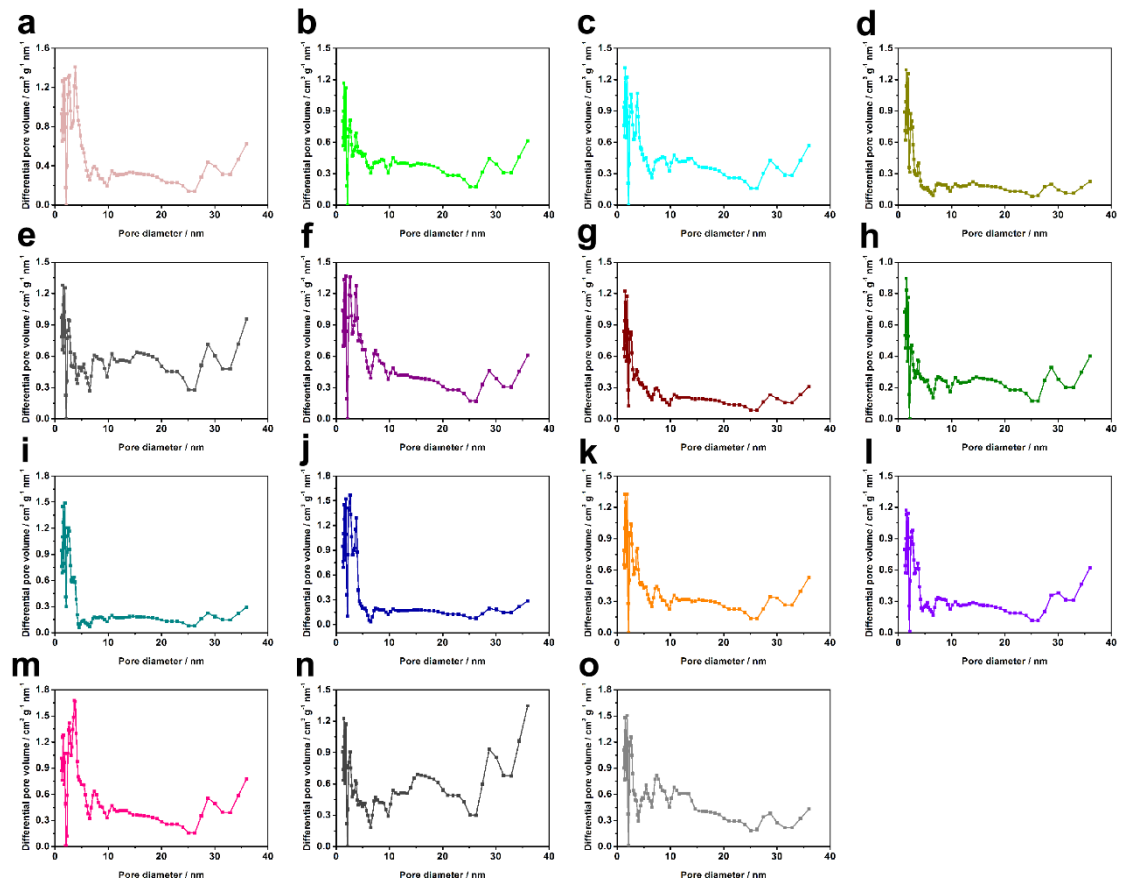


Fig. S13 Pore size distributions of hierarchically porous heteroatom-doped carbon materials derived from (a) cirsium setosum leaves, (b) lavender flowers, (c) mother chrysanthemum leaves, (d) stigma of corn, (e) bamboo fungus, (f) felon herb, (g) rabdosia rubescens stems, (h) rhus typhina fruit, (i) kowkui leaves, (j) loofah fruit, (k) mother chrysanthemum flowers, (l) peanut leaves, (m) honeysuckle flowers, (n) chili and (o) malachium aquaticum leaves.

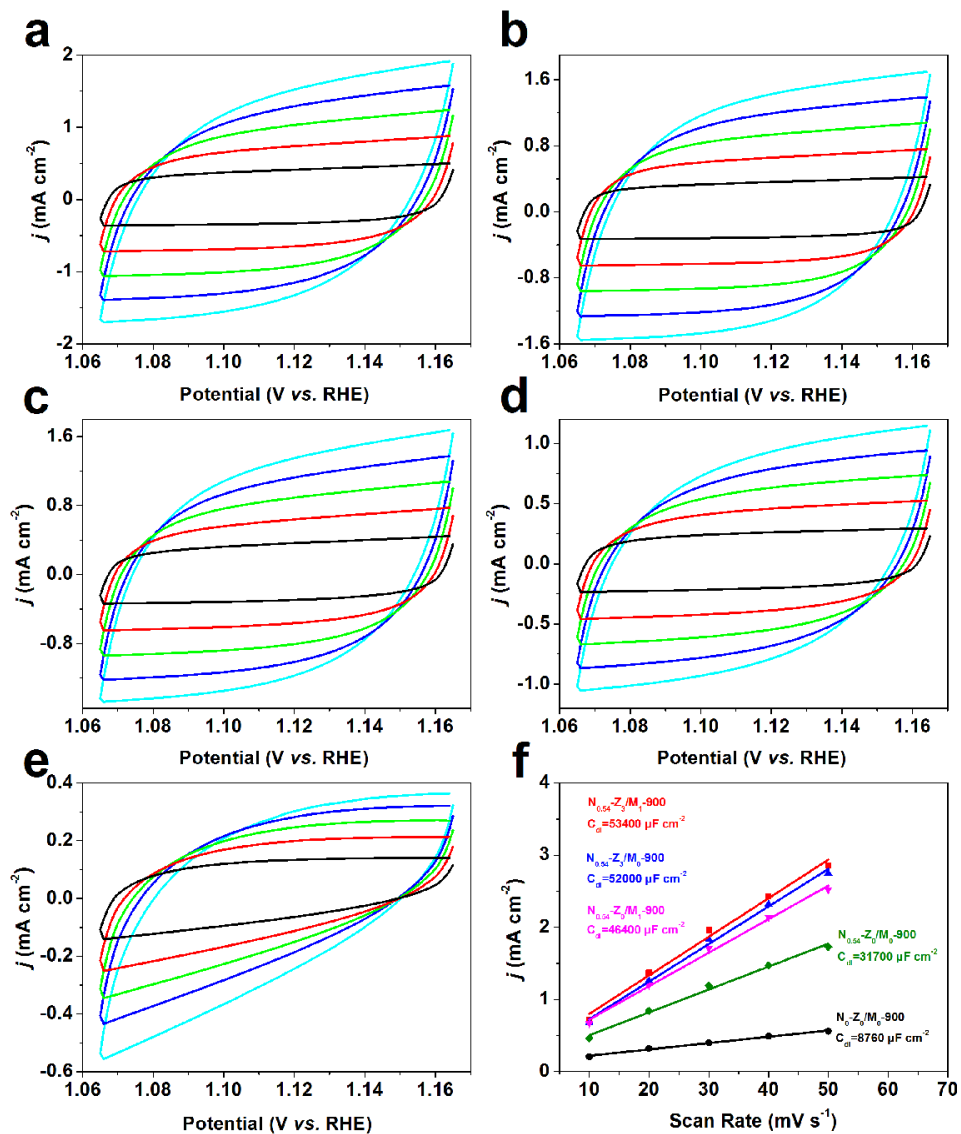


Fig. S14 CV curves of (a) $\text{N}_{0.54}\text{-Z}_3/\text{M}_1\text{-900}$, (b) $\text{N}_{0.54}\text{-Z}_3/\text{M}_0\text{-900}$, (c) $\text{N}_{0.54}\text{-Z}_0/\text{M}_1\text{-900}$, (d) $\text{N}_{0.54}\text{-Z}_0/\text{M}_0\text{-900}$ and (e) $\text{N}_0\text{-Z}_0/\text{M}_0\text{-900}$ modified electrodes in the double-layer region at scan rates of 10, 20, 30, 40 and 50 mV s^{-1} in 0.1 M KOH aqueous electrolyte; (f) current density (taken at the potential of 1.115 V) as a function of scan rate derived from (a) to (e).

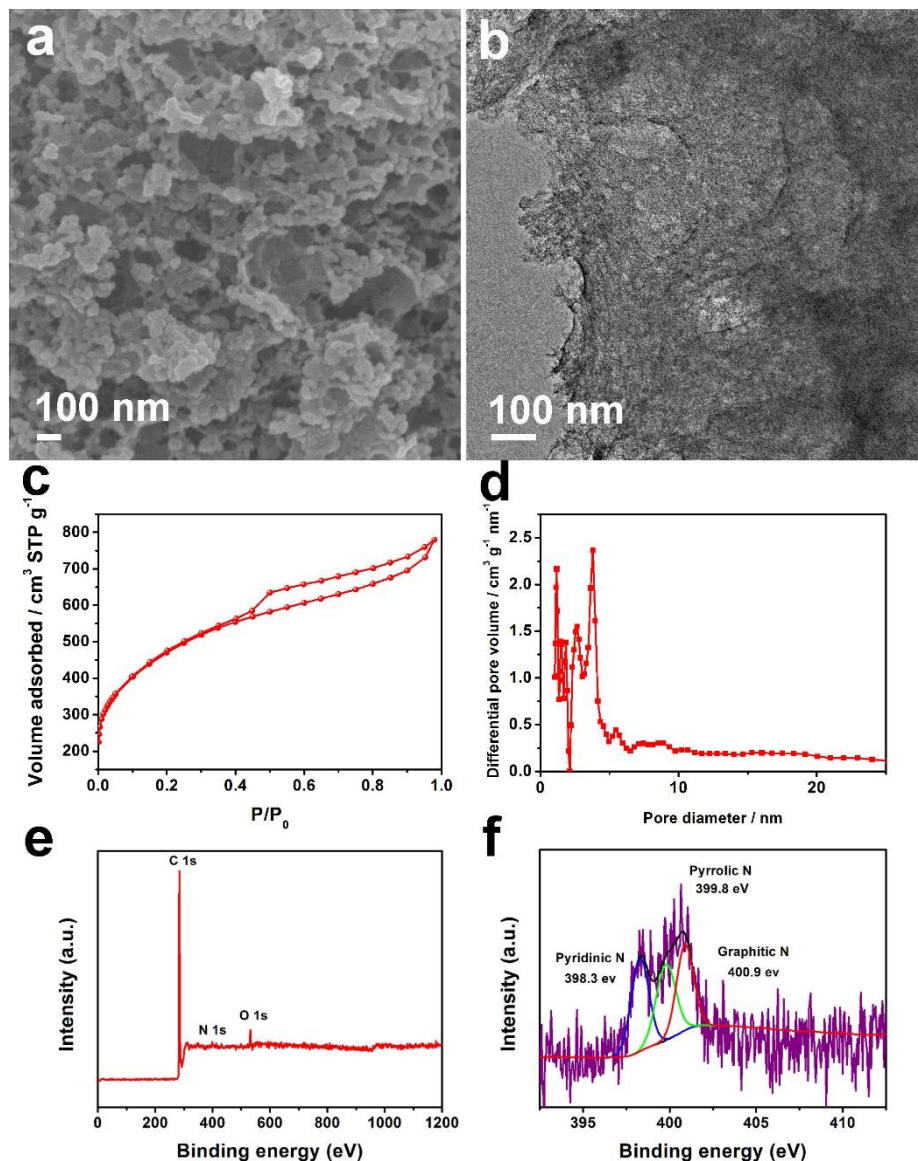


Fig. S15 (a) FESEM image, (b) TEM image, (c) N_2 sorption isotherms, (d) pore size distribution, (e) XPS survey and (f) N 1s spectra of $\text{N}_{0.27}\text{-Z}_3\text{/M}_1\text{-900}$.

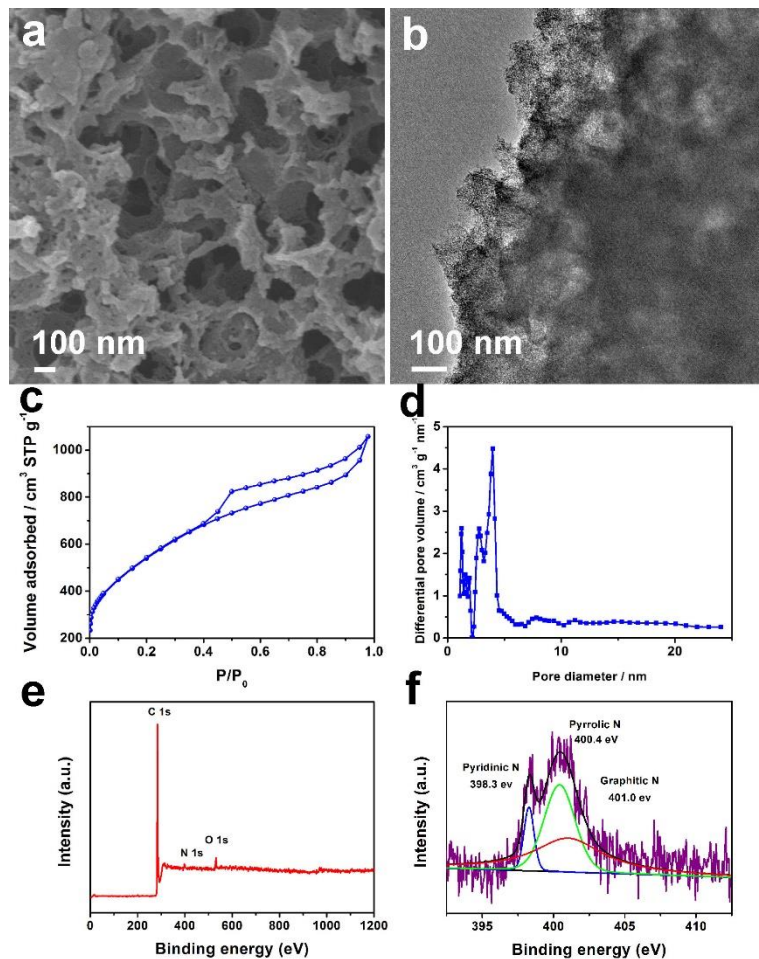


Fig. S16 (a) FESEM image, (b) TEM image, (c) N_2 sorption isotherms, (d) pore size distribution, (e) XPS survey and (f) N 1s spectra of $N_{1.05}\text{-}Z_3\text{/}M_1\text{-}900$.

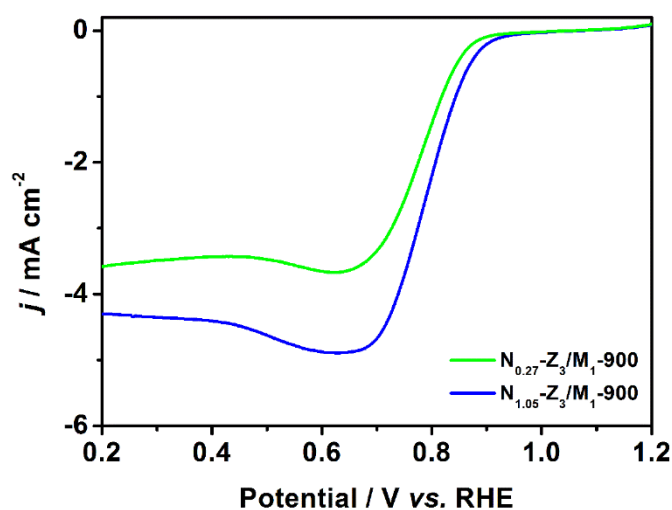


Fig. S17 LSV curves of $N_{0.27}\text{-}Z_3\text{/}M_1\text{-}900$ and $N_{1.05}\text{-}Z_3\text{/}M_1\text{-}900$.

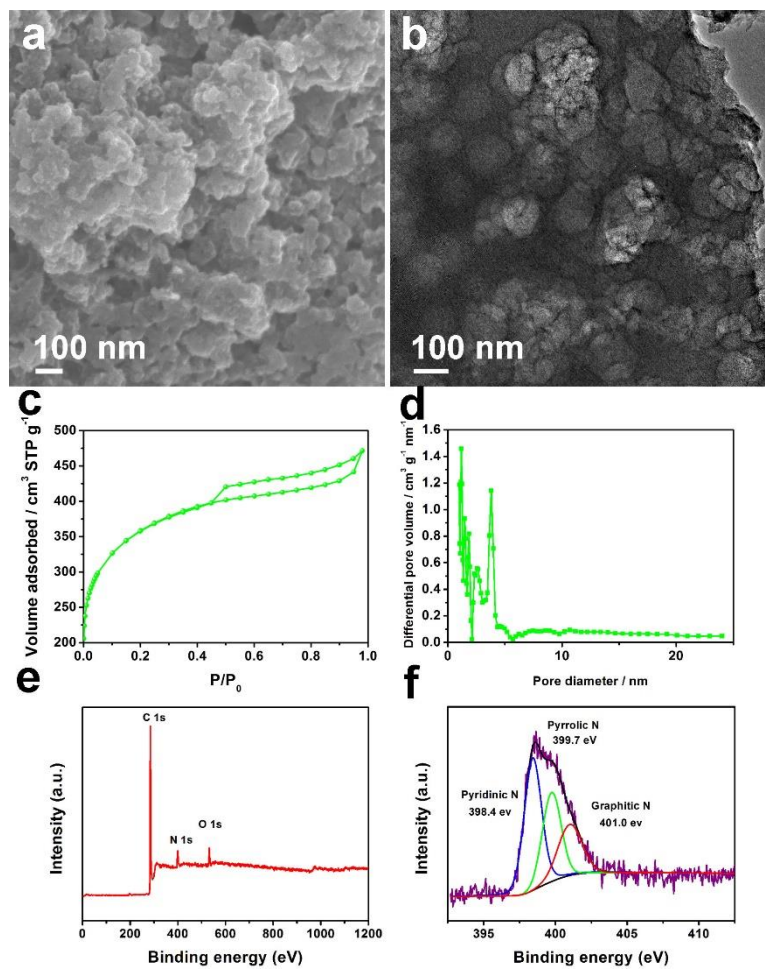


Fig. S18 (a) FESEM image, (b) TEM image, (c) N_2 sorption isotherms, (d) pore size distribution, (e) XPS survey and (f) N 1s spectra of $\text{N}_{0.54}\text{-Z}_3/\text{M}_{0.5}\text{-900}$.

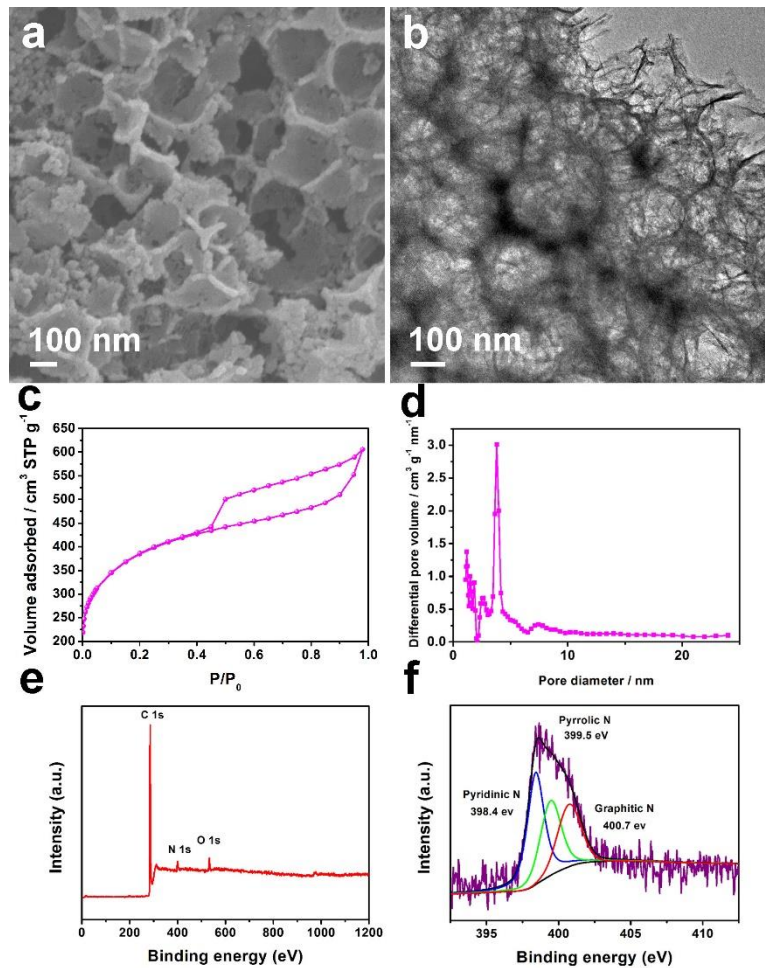


Fig. S19 (a) FESEM image, (b) TEM image, (c) N_2 sorption isotherms, (d) pore size distribution, (e) XPS survey and (f) N 1s spectra of $\text{N}_{0.54}\text{-Z}_3\text{/M}_{1.5}\text{-900}$.

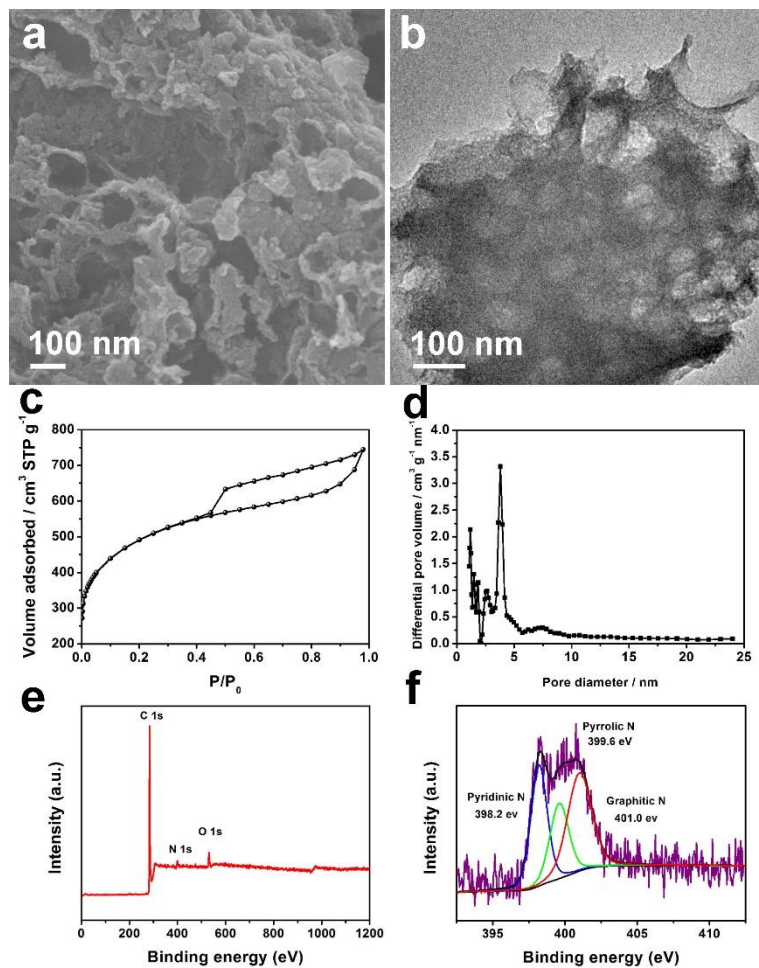


Fig. S20 (a) FESEM image, (b) TEM image, (c) N_2 sorption isotherms, (d) pore size distribution, (e) XPS survey and (f) N 1s spectra of $\text{N}_{0.54}\text{-Z}_2\text{/M}_1\text{-900}$.

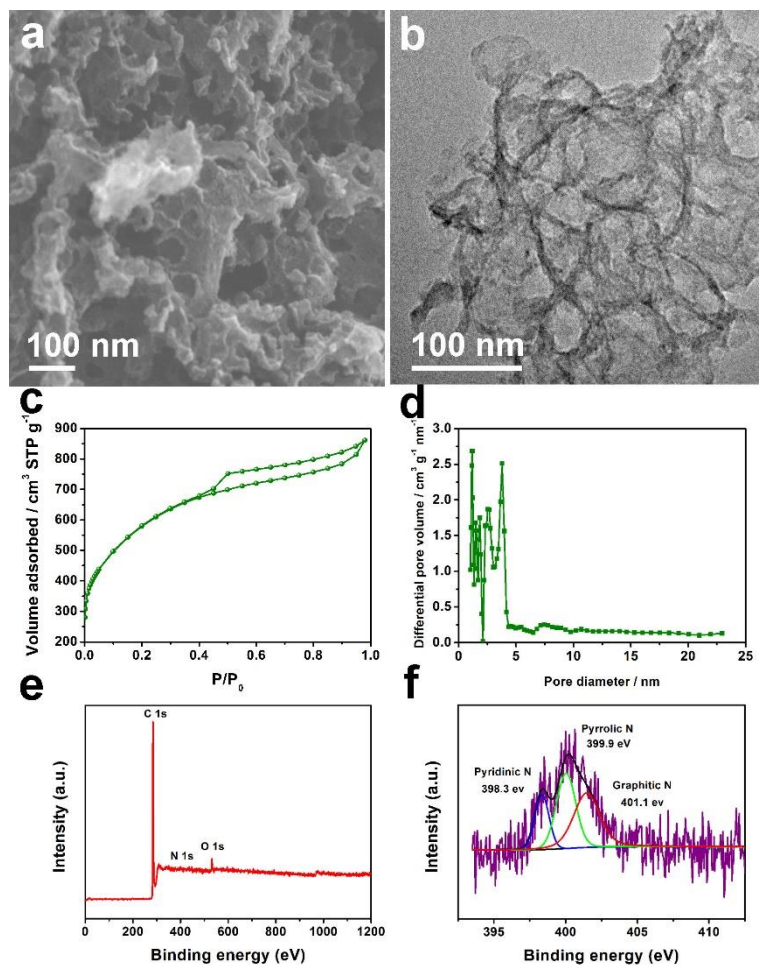


Fig. S21 (a) FESEM image, (b) TEM image, (c) N_2 sorption isotherms, (d) pore size distribution, (e) XPS survey and (f) N 1s spectra of $N_{0.54}\text{-}Z_4\text{/}M_1\text{-}900$.

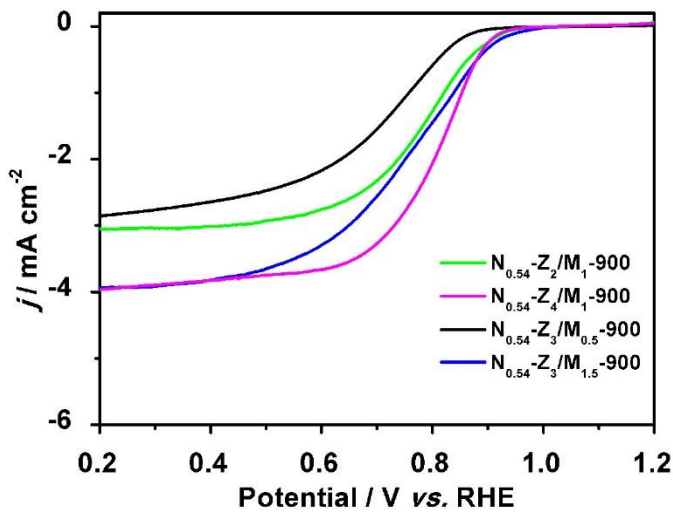


Fig. S22 LSV curves of $N_{0.54}-Z_3/M_{0.5}-900$, $N_{0.54}-Z_3/M_{1.5}-900$, $N_{0.54}-Z_2/M_1-900$ and $N_{0.54}-Z_4/M_1-900$.

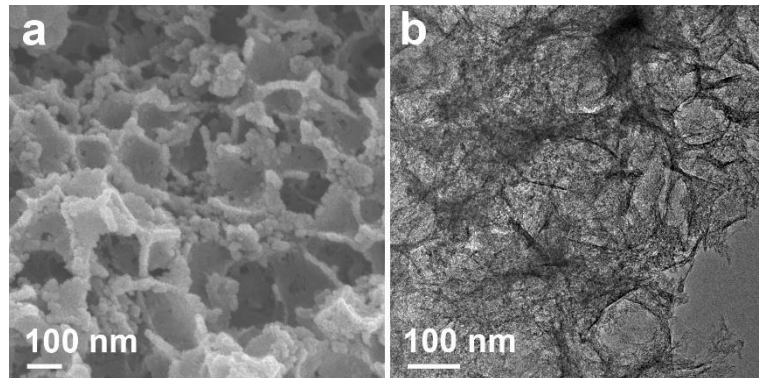


Fig. S23 (a) FESEM and (b) TEM images of the $N_{0.54}-Z_3/M_1-900$ sample after the stability test for 24 h.

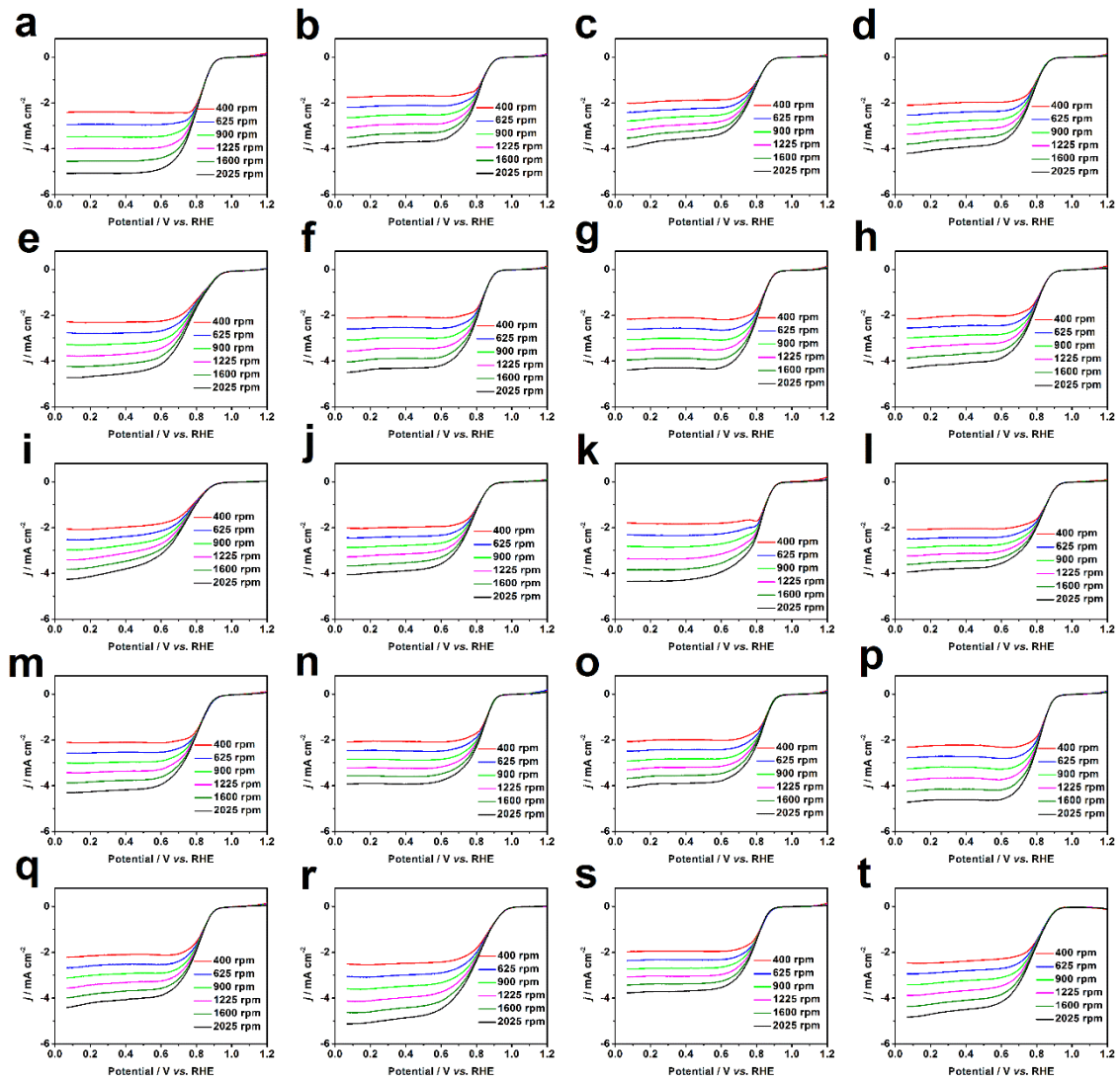


Fig. S24 LSV curves of hierarchically porous heteroatom-doped carbon materials derived from (a) carrots, (b) Chinese yam stems, (c) ginkgo leaves, (d) tung flowers, (e) long beans, (f) cirsium setosum leaves, (g) lavender flowers, (h) mother chrysanthemum leaves, (i) stigma of corn, (j) bamboo fungus, (k) felon herb, (l) rhabdosia rubescens stems, (m) rhus typhina fruit, (n) kowkui leaves, (o) loofah fruit, (p) mother chrysanthemum flowers, (q) peanut leaves, (r) honeysuckle flowers, (s) chili and (t) malachium aquaticum leaves.

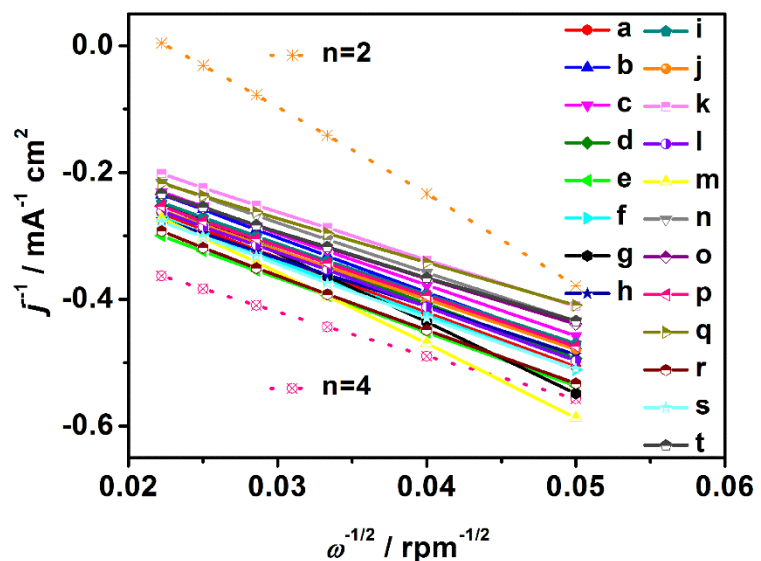


Fig. S25 Koutecky-Levich plots (j^{-1} vs. $\omega^{-1/2}$) from the LSV curves (Fig. S24) of hierarchical porous heteroatom-doped carbon materials derived from (a) carrots, (b) Chinese yam stems, (c) ginkgo leaves, (d) tung flowers, (e) long beans, (f) cirsium setosum leaves, (g) lavender flowers, (h) mother chrysanthemum leaves, (i) stigma of corn, (j) bamboo fungus, (k) felon herb, (l) rabdosia rubescens stems, (m) rhus typhina fruit, (n) kowkui leaves, (o) loofah fruit, (p) mother chrysanthemum flowers, (q) peanut leaves, (r) honeysuckle flowers, (s) chili and (t) malachium aquaticum leaves.

Table S1. Structural and compositional information and electrocatalytic performance of different N_x-Z_y/M_z-T samples.

Sample	S _{BET} ^a (m ² g ⁻¹)	V _{total} ^b (ml g ⁻¹)	d _{average} ^c (nm)	N content ^d (at.%)	V _{onset} ^e (V)	V _{half-wave} ^f (V)	j ^g (mA cm ⁻²)
N ₀ -Z ₀ /M ₀ -900	630	0.28	1.78	0	0.78	0.574	1.8
N _{0.54} -Z ₀ /M ₀ -900	420	0.22	2.12	1.24	0.90	0.620	1.7
N _{0.54} -Z ₀ /M ₁ -900	797	1.00	5.05	2.98	0.91	0.806	3.0
N _{0.54} -Z ₃ /M ₀ -900	1255	0.76	2.43	2.89	0.94	0.820	3.3
N _{0.54} -Z ₃ /M ₁ -900	1394	0.96	2.77	3.62	0.94	0.824	4.3
N _{0.27} -Z ₃ /M ₁ -900	1689	1.20	2.86	1.56	0.92	0.784	3.6
N _{1.05} -Z ₃ /M ₁ -900	1952	1.64	3.36	3.66	0.93	0.800	4.3
N _{0.54} -Z ₃ /M _{0.5} -900	1314	0.73	2.22	3.48	0.90	0.714	2.8
N _{0.54} -Z ₃ /M _{1.5} -900	1392	0.93	2.70	3.04	0.94	0.753	3.9
N _{0.54} -Z ₂ M ₁ -900	1371	1.15	2.61	2.96	0.94	0.778	3.1
N _{0.54} -Z ₄ M ₁ -900	2077	1.33	2.57	3.28	0.94	0.806	3.9

^a BET specific surface area. ^b Total pore volume. ^c Average pore diameter. ^d Nitrogen content. ^e Onset potential. ^f Half-wave potential. ^g Diffusion-limited current.

Table S2. Structural and compositional information and electrocatalytic performance of hierarchically porous heteroatom-doped carbon materials derived from different biomass precursors.

Precursors	S _{BET} ^a (m ² g ⁻¹)	V _{total} ^b (cm ³ g ⁻¹)	d _{average} ^c (nm)	N content ^d (at.%)	V _{onset} ^e (V)	V _{half-wave} ^f (V)	j ^g (mA cm ⁻²)
Carrot	1630	1.68	4.14	2.92	0.94	0.783	4.5
Chinese yam stem	1548	1.27	3.29	2.78	0.93	0.803	3.5
Ginkgo leaves	1366	1.25	3.66	2.25	0.93	0.768	3.5
Tung flower	1316	1.08	3.29	1.89	0.92	0.764	3.7
Long bean	1517	1.45	3.83	2.82	0.98	0.774	4.2
Cirsium setosum	1548	1.32	3.41	2.53	0.94	0.807	4.0
Lavender	1358	1.19	3.52	2.57	0.95	0.807	3.9
Mother chrysanthemum leaves	1492	1.28	3.43	3.16	0.94	0.780	3.8
Stigma of corn	1451	0.97	2.68	1.06	0.94	0.729	3.8
Bamboo fungus	1466	1.27	3.47	2.73	0.93	0.768	3.6
Felon herb	1621	1.42	3.52	1.5	0.94	0.818	3.8
The stems of rhabdosia rubescens	1426	1.01	2.85	2.59	0.95	0.809	3.6
The fruits of rhus typhina	1049	0.84	3.22	2.71	0.95	0.792	3.8
Kowkui	1679	1.11	2.66	2.48	0.95	0.827	3.5
Loofah	1752	1.20	2.74	2.61	0.94	0.820	3.6
Mother chrysanthemum	1548	1.24	3.20	2.61	0.95	0.811	4.2
Peanut leaf	1390	1.12	3.22	0.66	0.94	0.795	4.0
Honeysuckle	1548	1.24	3.20	1.79	1.01	0.806	4.6
Chili	1459	1.49	4.10	2.45	0.93	0.789	3.4
Malachium aquaticum	1734	1.43	3.30	2.95	0.96	0.773	4.3

^a BET specific surface area. ^b Total pore volume. ^c Average pore diameter. ^d Nitrogen content. ^e Onset potential. ^f Half-wave potential. ^g Diffusion-limited current.

Table S3. Summary of various carbon-based electrocatalysts for ORR.

Catalysts	V_{onset}^a (V)	$V_{\text{half-wave}}^b$ (V)	j^c (mA cm $^{-2}$)	References
N _{0.54} -Z ₃ /M ₁ -900	0.96	0.825	4.3	This study
N-graphene	0.77	NA	0.8	<i>ACS Nano</i> 2010 , <i>4</i> , 1321
Undoped CNT	0.92	NA	4.5	<i>J. Am. Chem. Soc.</i> 2011 , <i>133</i> , 5182
Intrinsic carbon	0.88	NA	NA	<i>ACS Catal.</i> 2015 , <i>5</i> , 6707
N-doped carbon	0.86	0.70	4.6	<i>Energy Environ. Sci.</i> 2014 , <i>7</i> , 442
Zigzag-type graphene	0.96	0.819	4.8	<i>Adv. Mater.</i> 2018 , <i>30</i> , 3819
N/S co-doped carbon	0.86	0.75	5.1	<i>Adv. Funct. Mater.</i> 2016 , <i>26</i> , 5893
N-S-doping porous carbons	0.87	0.74	5.5	<i>Adv. Funct. Mater.</i> 2016 , <i>26</i> , 8651
N, S doped graphene	0.90	NA	NA	<i>Angew. Chem. Int. Ed.</i> 2012 , <i>51</i> , 11496
C ₃ N ₄ /carbon	0.82	NA	NA	<i>Angew. Chem. Int. Ed.</i> 2012 , <i>51</i> , 3892
Macro/meso-NC-NH ₃	NA	0.82	6.6	<i>Energy Environ. Sci.</i> 2015 , <i>8</i> , 3274
Porous carbon	0.94	0.85	4.2	<i>Nat. Nanotechnol.</i> 2015 , <i>10</i> , 444
Hierarchically porous carbon	0.96	0.84	5.2	<i>ACS Catal.</i> 2017 , <i>7</i> , 6082

^aOnset potential. ^bHalf-wave potential. ^cDiffusion-limited current.